

Multiscale phase oscillations induced by cluster synchronisation in human connectome core network

Bosiljka Tadić^{1,2,3}, Marija Mitrović Dankulov², Roderick Melnik^{4,5}

¹*Department of Theoretical Physics, Jožef Stefan Institute, Jamova 39, Ljubljana, Slovenia*

²*Institute of Physics, Pregrevica 118, 11080 Belgrade, Serbia*

³*Complexity Science Hub Vienna, Metternichgasse 8, 1030 Vienna, Austria*

⁴*MS2Discovery Interdisciplinary Research Institute; M3AI Laboratory and Department of Mathematics, Wilfrid Laurier University, Waterloo, ON, Canada and*

⁵*BCAM - Basque Center for Applied Mathematics; Alameda de Mazarredo 14, E-48009 Bilbao Spain*
(Dated: July 11, 2025)

Brain imaging data mapping onto human connectome networks enables the investigation of global brain dynamics, where the brain hubs play an essential role in transferring activity between different brain parts. At this scale, the synchronisation processes are increasingly investigated as one of the key mechanisms revealing many aspects of brain functional coherence in healthy brains and revealing deviations due to various brain disorders. For the human connectome core network, consisting of the eight brain hubs and the higher-order structure attached to them, previous simulations of Kuramoto phase oscillators at network nodes indicate instability of the global order parameter for a range of positive coupling strengths. In this work, we investigate the multiscale oscillations of the global phase order parameter and show that they are connected with the cluster synchronisation processes occurring in this range of couplings below the master stability threshold. We use the spectral graph analysis and eigenvector localisation methodology, where the clusters of nodes playing a similar role in the synchronisation processes have a small mutual distance in the eigenvector space. We determine three significant clusters of brain regions and show the position of hubs in them. With the parallel analysis of the weighted core network and its binary version, we demonstrate the primary role of the network's topology in the formation of synchronised clusters. Meanwhile, the weights of edges contribute to the hub's synchronisation with the surrounding cluster, stabilise the order parameter variations and reduce the multifractal spectrum.

I. INTRODUCTION

The Human connectome (HC) structure representing the large-scale brain networks is nowadays readily available from the brain-imaging data¹ mapped to network structures. The nodes are identified as the anatomical brain regions and the edges represent neuron bundles connecting them. Integrated complex mapping procedures including the parcellation, tractography, and graph construction, are now available subject to various selection of parameters; see, for example, the Budapest connectome server^{2,3} for details. Advances in the knowledge of HC structure allowed investigation of global brain dynamics⁴⁻⁶. In different processes associated with the HC, the brain hubs⁷ as the best connected central nodes play an essential role in transferring the activity between different brain parts and the formation of co-activated groups of regions, bridging between anatomical and functional features⁸. It has been recognised how the hub's fragility⁹ and "disturbances of their structural and functional connectivity profile are linked to neuropathology"¹⁰. Hence, the current research efforts focus on hubs-supported pathways in the brain function; see, for example, studies in ref.¹¹ stating that "Understanding the concept of network hubs and their role in brain disease is now rapidly becoming important for clinical neurology".

Based on identified brain networks, the higher-order structures described by simplicial complexes, have been determined in the consensus human connectomes¹². See also homological scaffold study in¹³. The higher-order cortical connectivity is generally investigated as enabling reliable and efficient neural coding¹⁴. Higher-order structures are increasingly considered in the context of human brain functionality and, in particular, the appearance and classification of various brain disorders^{5,15}. In the human connectome network, the brain hubs appear mutually connected, representing a rich-club structure¹⁶. Moreover, the eight hubs hold the leading higher-order structures reaching different brain parts, thus representing the *core of the human connectome* structure. In ref.¹⁷, the HC core network was determined by identifying simplexes of all orders attached to (at least one of) the brain hubs. See detailed description below in Sec. II.

Synchronization on human connectome has been studied as one of the key processes of functional properties at the whole-brain scale, revealing the degree of collective dynamic behaviour in the interplay with the complex connectome's topology¹⁸. In this context, the use of a simple Kuramoto model with the oscillators associated with the network nodes and influencing each other along the weighted edges are widely accepted both in the theoretical consideration as well as the empirical data evaluation^{19,20}. In computational neuroscience, it has been recognised that the occurrence of synchronised clusters¹⁹ rather than the whole connectome synchrony corresponds to natural dynamical states in healthy brain functions supporting the emotion, cognition and behaviours; in contrast, the alternation of the functional connectivity and related patterns of partial synchrony can be connected to specific types of brain disorders, neurologic and psychiatric processes²⁰.

Cluster synchronisation in complex networks has been investigated in relation to the functional properties of networks and

their applications in neurology and other science disciplines^{19,21–24}. Theoretically, in transition to a fully synchronised state, different clusters consisting of roughly synchronised nodes have different evolution patterns when the global coupling strength is below the master stability point; above this point, mutual synchronisation among different clusters occurs, leading to the complete network synchrony; see²⁵ and references there for detailed consideration. Methodologically, clusters of nearly synchronised nodes are determined using the spectral analysis of the Laplacian operator associated with the underlying network structure²². The methodology is based on the localisation of the eigenvectors of the sequence of smallest nonzero eigenvalues of the Laplacian, utilising the idea that nodes at “symmetrical” positions in the network, i.e., having a vanishing distance in the eigenvectors space, are playing a similar role in the synchronisation processes. See Section III for a more detailed description.

Building on the previous results in ref.²⁶, we study the cluster synchronisation properties of the human connectome core network and their impact on the modulation of temporal dynamics of the global synchronisation order parameter. Using the methodology of the Laplacian spectral analysis, we demonstrate the occurrence of cluster synchronisation in a range of positive couplings associated with the observed order parameter instability, and determine three leading clusters around the brain hubs. A parallel analysis of the core network with the natural weights and its binary version reveals the primary role of topology and the stabilising impact of the weight of the edges. These cluster-synchronisation patterns dynamically impact the multiscale fluctuations of the global order parameter, which we study using the appropriate multifractal analysis.

The paper is organised as follows. In Section II, we present details regarding the network structure, its spectral analysis, and the results of synchronisation dynamics from²⁶ that are relevant to this work. Furthermore, in Section III, we apply the cluster-synchronisation methodology and determine the major cluster both in the weighted HC core network and its binary version. Section IV presents the multifractal analysis of the temporal fluctuations of the order parameter inside the instability region of both weighted and binary network versions. Final Section V briefly summarises and discusses the results.

II. HUMAN CONNECTOME CORE NETWORK AND ITS SYNCHRONISATION PROPERTIES

In this section, we give a more precise definition of the human connectome core network and present its structural properties with the results of its spectral analysis. Furthermore, as stated in the Introduction, we consider its synchronisation properties to elucidate the role of hubs in the appearance of clusters and their dynamic consequences. We show the results of the phase synchronisation of Kuramoto oscillators on this network²⁶ that motivate our study of cluster synchronisation.

1. The human connectome core network

The core connectome network is determined¹⁷ as a part of the human connectome associated with the brain hubs L. Caudate, L. Putamen, L. Thalamus-Proper, L. Hippocampus in the Left and the corresponding Right hemisphere nodes. Specifically, we use the HC core network shown in Fig. 1, which is extracted from the consensus male connectome determined in¹² based on the brain imaging data from the Budapest human connectome server^{2,3}. The network consists of eight brain hubs and nodes (brain regions) that make simplexes of all orders associated with these hubs. Fig. 1 displays the structure of connections associated with the brain hubs (big nodes) and weighted edges, where the weights are determined according to the electrical connectivity criteria as the number of fibres tracked between a pair of brain regions normalised by the average fibre length between them (see¹² for details).

The distribution of weights in this HC core network is shown in the inset of Fig. 2, indicating a broad range of weights. Apart from the small weights, the data can be fitted by the \tilde{q} -Gaussian²⁷ distribution $f(x) = a \left[1 - (1 - \tilde{q})(x/b)^2 \right]^{1/1-\tilde{q}}$, where we find $\tilde{q} \lesssim 2$. As shown in ref.¹⁷, all nodes and edges in the male core connectome also exist in the consensus female connectome, but with slightly different weights on the edges. A detailed analysis of the higher-order connectivity using the simplicial complexes representation of both female and male connectome and the corresponding core networks can be found in refs.^{12,17}.

2. Eigenvalues spectrum of the human connectome network

We focus on the spectral analysis of the Laplacian operator associated with the human connectome networks (1-skeleton of the simplicial complex), motivated by the theoretical background connecting the eigenvalue spectrum of the network structure with the diffusive dynamics on it²⁹. Specifically, we determine the eigenvalues λ_i , $i = 1, 2 \dots N$, and the corresponding eigenvectors v_i of the Laplacian of weighted and binary networks. For convenience, we consider the positive-definite Laplace operator, whose matrix elements $L_{ij} \equiv -\Delta_{ij}$ are given by

$$L_{ij} = S_i \delta_{ij} - W_{ij} \quad (1)$$

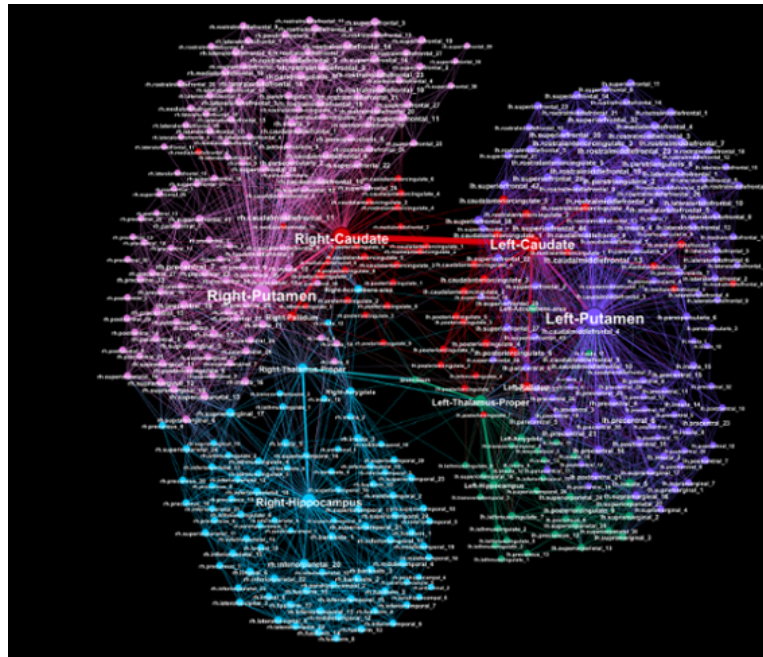


FIG. 1: The weighted undirected Human Connectome core network comprising the eight brain hubs and associated simplexes, with the weights on edges extracted from the consensus male connectome; data are from¹⁷. it contains $N = 418$ nodes and $E = 3835$ edges. The node's labels represent the anatomical brain area, the node's size is proportional to its degree, and colours indicate different topological communities. Graph visualisation using *gephi*²⁸.

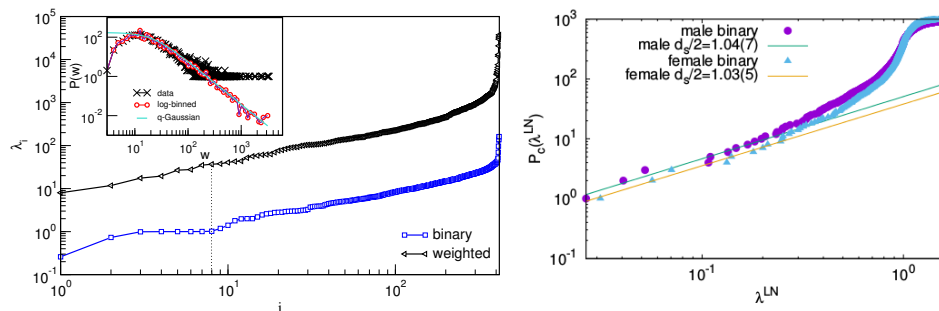


FIG. 2: Left panel shows the nonzero eigenvalues λ_i , $i = 1, 2, \dots, 417$ in ranking order for the HC core network in Fig. 1. The distribution of weights of edges shown in the inset panel is fitted by q -Gaussian with $q = 1.9 \pm 0.11$; the data are from ref.¹⁷. The right panel shows the cumulative distribution $P_c(\lambda^{LN})$ of the eigenvalues λ^{LN} of the normalised Laplacian operator for the whole consensus human connectomes. The fitted regions for small λ values determine the spectral dimension $d_s/2$.

where $W_{ij} > 0$ indicates the presence and the actual weight of the edge (i, j) and $S_i = \sum_{l=1}^N W_{il}$ is the node's strength. To differentiate the impact of weights of the edges compared to the global topology of the network in its synchronisation features, we analyse in parallel the binary version of the HC core network, in which W_{ij} is replaced by the adjacency matrix elements $A_{ij} = 1$ for each (i, j) pair where the edges exist, and zero otherwise. Consequently, the $S_i \rightarrow k_i$ becomes the node's degree. The main panel in Fig.2 left shows the eigenvalues of the Laplacian (1) for both the weighted core network, Fig. 1, and its binary version. The eigenvalues are shown in the ranking order with $\lambda_0 = 0 < \lambda_1 \leq \lambda_2 \leq \lambda_3 \leq \dots \leq \lambda_{N-1}$, where the equality applies for the eigenvalue degeneracy. This figure shows the differences between weighted and binary network spectra that affect their cluster synchronisation. In particular, a range of small eigenvalues (up the vertical dotted line) and their eigenvectors play a key role in the cluster synchronisation properties, as shown in Section III. Before studying the cluster synchronisation in detail, we demonstrate that the structure of the human connectome networks is suited for partial synchronisation, featuring the spectral dimension $d_s \geq 2$. In the right panel of Fig. 2, we show the cumulative distribution of human connectome networks (consensus male and female networks). In this case, we use the normalised³⁰ version of the Laplacian (1), whose components are $L_{ij}^{LN} = \delta_{ij} - \frac{A_{ij}}{\sqrt{k_i k_j}}$ for the case of binary networks. The cumulative distribution $P_c(\lambda)$ shows a scaling behavior $P_c(\lambda) \simeq \lambda^{d_s/2}$

in the range of small nonzero eigenvalues. The scaling exponent $d_s/2$ determines the network's spectral dimension d_s , which signifies the impact of the network structure on the nature of stochastic dynamics on it; see, for example, references^{31,32} and references there. Here, we find that the spectral dimension of the human connectome networks is close to $d_s = 2.1$ within the numerical error bars. The spectral dimensions in this range are found in the networks of self-assembled cliques of various dimensions in ref.³⁰, suggesting a specific type of simplicial architecture with geometrically constrained aggregation. According to the studies of network synchronisation, the structures with these spectral dimensions can not support thermodynamically stable synchronised phases³². Thus, the occurrence of dynamical patterns with partial synchronisation is most probable. Moreover, the components of the eigenvectors v_{ik} of the smallest nonzero eigenvalues of the Laplacian localise to the underlying network communities and are efficiently utilised for the community detection^{33,34}. Recently, these spectral methods also gained attention in Data science and Machine learning literature^{35,36}. Fig. 1 shows that the considered human connectome core network exhibits a community structure. These communities appear to affect the cluster synchronisation patterns, as shown in the next section.

3. Synchronisation of phase oscillators on human connectome core networks

Simulations of synchronisation processes that we use in this work are done in ref.²⁶ considering Kuramoto oscillators with the phase θ_i , $i = 1, 2, \dots, N$, defined as an angle on a unit circle, associated with the nodes of the core network in Fig. 1, and interacting via the network's edges. The coupled equations govern the evolution of the node's phases

$$\dot{\theta}_i = \omega_i + \frac{K_1}{\sum_{l=1}^N W_{il}} \sum_{j=1}^N W_{ij} \sin(\theta_j - \theta_i) \quad (2)$$

where K_1 is the global coupling strength; the intrinsic frequency of the i -th oscillator ω_i is taken from Gaussian distribution and kept fixed during the simulation time. We note that the equation (2) takes into account the actual weights of the edges via W_{ij} matrix elements and the normalisation factor, corresponding to the strength of the node $S_i \equiv \sum_{l=1}^N W_{il}$. As stated above, in the network's binary version, these factors are replaced by the adjacency matrix and the node's degree, respectively. The network synchronisation properties are studied in the literature by varying the global coupling strength K_1 from significant negative to large positive values. See also^{37,38} for synchronisation of Kuramoto oscillators on simplicial complexes with different architecture and simplex-embedded higher-order interactions.

A suitable measure of the collective synchronisation level is the Kuramoto order parameter r defined as

$$r = \left\langle \left| \frac{1}{N} \sum_{j=1}^N e^{i\theta_j} \right| \right\rangle \quad (3)$$

where $\langle \cdot \rangle$ indicates the time average over a large number of simulation steps suitably chosen after a long transient interval. For the simulation details, see ref.²⁶. We note that when a pattern of partial synchronisation occurs, the global order parameter may have finite values $0 < r < 1$ between the completely desynchronised phases, where $r \rightarrow 0$, and full synchrony $r \rightarrow 1$, which can be reached for $K_1 > 0$ asymptotically when the global coupling $K_1 \rightarrow \infty$. Fig.3 shows the results for the order parameter for the phase synchronisation obtained in ref.²⁶ on the above-described human connectome core network, Fig.1, and its binary version. This figure shows that both weighted and binary networks exhibit instability in the region of positive couplings K_1 , here denoted as $[K_1^-, K_1^+]$, where the (time and sample) averaged order parameter fluctuates. Such instability occurs for a range of small coupling strengths $K_1 > 0$, before the full synchrony is reached asymptotically at substantial K_1 values. Notably, this instability is more pronounced in the case of binary structure than in the real weighted network. Based on the temporal evolution of individual node's phases studied in²⁶, we can identify the lower bound K_1^- where the nontrivial grouping of the evolution paths first occurs. We then follow the cluster aggregation until three major clusters eventually emerge, which mutually coordinate their evolution above the upper boundary K_1^+ . (The whole video of the simulations in²⁶ is available online <https://youtu.be/E9nFrXuoplk> for the range $K_1 \in [-30, 30]$ in small dK steps, where the starting state at $K_1 \rightarrow K + dK$ value is achieved for the preceding K_1 , the procedure is known as "tracking the attractor"³⁷). Hence, we can identify these bounds for the binary network as $[1.88, 7.2]$ within which we observe nonrandom fluctuations of the order parameter that will be associated with the cluster synchronisation, as shown below; meanwhile, the weighted edges lead to a more stable synchronisation pattern and shrinking the instability region, estimated as $[0.9, 4.2]$ for the original weighted network; see Section III.

In Fig. 4, the simulation data²⁶ of the phase evolution of individual nodes are shown to demonstrate the differences between the weighted network and its binary version; these data refer to the instability region, $K_1 = 2.399$ of both networks. Several groups of roughly synchronised nodes are visible in both cases, moving at different speeds. In the following section, we show the occurrence of synchronised clusters behind these temporal profiles. These evolution patterns lead to different temporal fluctuations of the global synchronisation order parameter, eq. (3), as shown in the lower panels of Fig. 4. Quantitative differences between these modulated oscillatory patterns of the order parameter are revealed by the multifractal analysis in section IV.

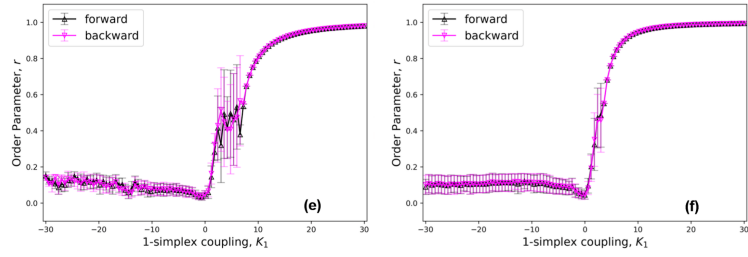


FIG. 3: Phase synchronisation order parameter r vs global coupling strength K_1 in HC core network. Data are part of fig2 in ref.²⁶.

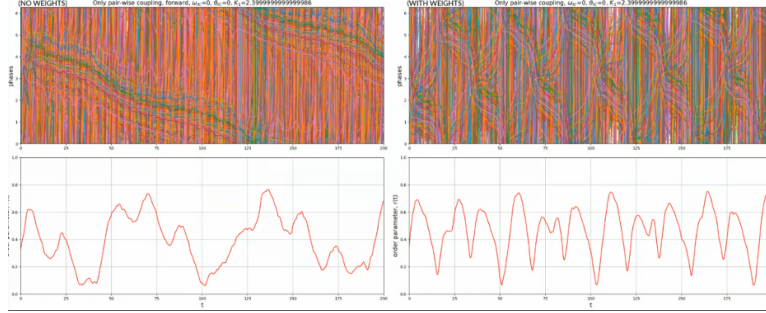


FIG. 4: Time evolution of phases of each node in the instability region for binary (left) and weighted HC core network (right); lower panels show the corresponding order parameter r vs time t in steps of 0.01; data are from Ref.²⁶.

III. CLUSTER SYNCHRONISATION IN HC-CORE NETWORK

As stated above, to determine synchronised clusters, we use the approach based on the localisation of the eigenvectors of the Laplacian operator (1) associated with the HC weighted core network, and also for its binary version described above. The corresponding eigenvalue spectra are shown in the left panel of Fig. 2 with the ordered eigenvalues $\lambda_0 < \lambda_1 \leq \lambda_2 \dots \leq \lambda_{N-1}$. As described in the literature, see, for example, ref.²⁴, this methodology resides on the idea of the master-stability threshold $g_c \equiv K_c \lambda_1$ for the global pairwise coupling K_c , above which the complete synchrony associated with the leading eigenvalue may emerge. Meanwhile, below g_c , the partial synchronisation can occur in terms of different clusters of nodes with almost identical evolution associated with the eigenvalue modes of $\lambda_0 < \lambda_1 \leq \lambda_2 \dots \leq \lambda_m$ orthogonal to the main synchronisation pattern²⁴. (Note that we restrict to the pairwise coupling; recently, the master-stability equation was generalised to consider simplexes larger than network edges in ref.³⁹.)

Assuming that the threshold $K_c = K_1^+$ associates with the upper bound of the instability region discussed above, then the sequence of modes corresponding to the eigenvalues λ_i is related to smaller values of the global coupling K_{1i} such that

$$K_{1i} = K_c \lambda_1 / \lambda_i \quad (4)$$

where $i = 2, 3, \dots, m$ until the lower bound is reached, i.e., $K_{1i} \geq K_1^-$. Thus, we determine the sequence of m eigenvalues that correspond to these unstable modes and their eigenvectors for both binary and weighted HC core network. Nodes that have the same projections of eigenvectors and, thus, a small distance in the space of eigenvectors corresponding to these modes are considered to belong to the same cluster. More precisely, for nodes i and j we can define distance

$$\delta e_{ij} = \sum_{k=1}^{m+1} |v_{ki} - v_{kj}| < \theta \quad (5)$$

where v_{ki} and v_{kj} are i and j components of the vector k that corresponds to k unstable mode. Ideally, $\theta = 0$; however, due to numerical precision limitation, a finite threshold is assumed, which we chose as $\theta = 0.003$, according to ref.²⁴.

Given the differences in the eigenvalue spectra, cf. Fig. 2, the number of unstable modes significantly differs in the weighted and binary networks. Precisely, we have $m = 8$ different modes in the weighted network; meanwhile, the eigenvalues $3 < i < 8$ are degenerate and only three first modes with different values contribute in the case of the binary network; cf. table III. With the equation (4) and the upper bound K_1^+ given above, these eigenvalues lead to the sequence of global couplings $K_{1i} = 2.551, 1.885, 1.867$ for $i = 2, 3, 4$ for the binary network. The corresponding values for the weighted network are 2.857, 1.918, 1.733, and so on; we have $K_{i=7} = 0.958$ and two more values above the lower bound identified as $K_1^- = 0.9$.

i	(binary)	weighted
1	0.25935471496502077	8.00624257944399
2	0.7319926928674106	11.766498485351391
3	0.9904154802265737	17.52885798614962
4	1.0000000000000195	19.519470842538514
5	1.0000000000000229	26.827478845152257
6	1.000511313383658	27.712076731684096
7	1.0047717952418098	35.09829539136315
8	1.020652012416054	36.86219625823234

The eigenvectors corresponding to these eigenvalues are shown in Fig. 5. Notably, most of the eigenvectors in this region of the spectra appear to localise on one or a couple of nodes; cf. Fig. 5 lower panel. Meanwhile, the eigenvectors v_1^B of the binary and v_7^W of the weighted network version are delocalised over four different network parts and the transition regions between them. Apart from more pronounced fluctuations of the eigenvector components in the case of v_7^W , the nodes and network regions where these eigenvectors have nonzero components are practically identical, suggesting the primary impact of topology in the eigenvector (de)localisation, cf. Fig. 5.

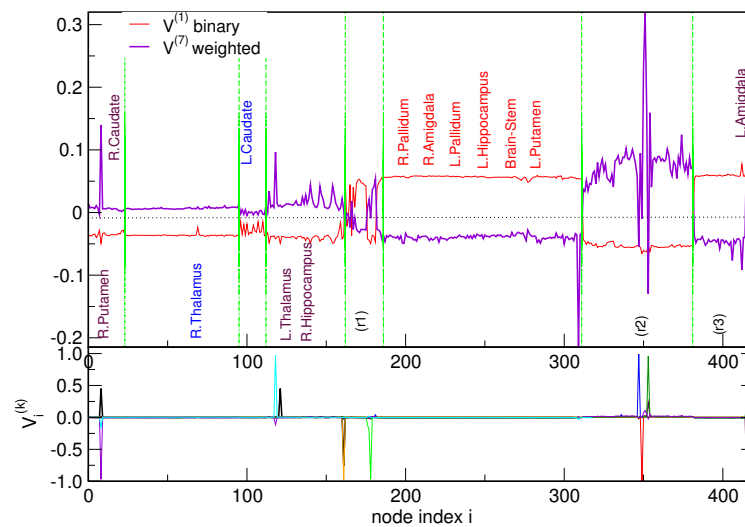


FIG. 5: The Laplacian eigenvectors of leading eigenvalues for the binary and weighted network localised on several nodes (lower panel) and two delocalised eigenvectors indicated in the legend (upper panel). Positions of the brain hubs are indicated; see text for more.

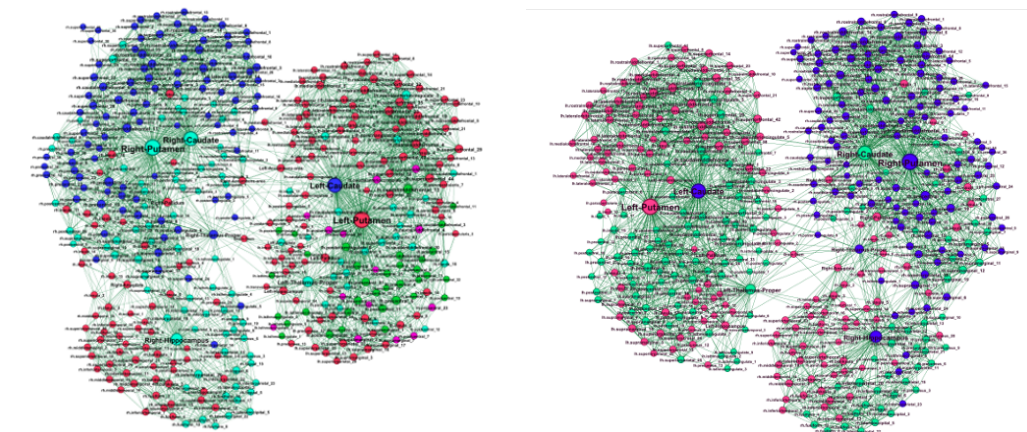


FIG. 6: The three most significant clusters (indicated by the blue, red and green colour of nodes) are identified across the instability region of the Human Connectome core network with the natural weights of the edges (right) and its binary version (left). All remaining nodes are shown in magenta. The size of nodes and their names (brain regions) are provided, scaled with the node's degree.

Furthermore, we determine synchronised clusters using the eq.(5) with the above-mentioned number of contributing eigenmodes in the weighted and binary network. Specifically, we find three large clusters and a number of small ones consisting of a few nodes and a certain number of nodes that do not belong to any of the clusters. In Fig. 6, we present the HC core binary and weighted networks with the identity of nodes belonging to three leading clusters shown in red, green and blue colour. All smaller clusters and unsynchronised nodes are shown in magenta colour. We note that apart from some hubs, the nodes belonging to these clusters in the weighted and binary network coincide to a large extent, which agrees with the eigenvector localisation in Fig. 5. Moreover, some hubs appear out of these clusters in the binary network, e.g., R.Putamen and R.Hippocampus; meanwhile, in the weighted network, they are synchronised with the surrounding blue and red clusters, respectively.

IV. MULTISCALE TEMPORAL FLUCTUATIONS IN THE CLUSTER-SYNCHRONISATION REGION

The occurrence of cluster synchronisation manifests in the modulations of the temporal evolution of the global order parameter r . We proceed with the multifractal analysis of the order-parameter time series for a coupling strength $K_1 = 2.399$ inside the instability region for the weighted and binary network; see lower panels of Fig. 4.

We use the multifractal analysis of time series^{40–45} to determine the nature of the OP fluctuations $r(t_k)$, for different datapoints $t_k = 1, 2, \dots, T_{max}$; in the simulations²⁶, $dt = 0.01$ such that the evolution time is $T_{max} = 20000$. We then use these multifractal properties to quantify the difference between the weighted and binary networks inside the instability region. The applied methodology utilises the self-similarity of the generalised fluctuation function $F_q(n)$ against the varying time interval n ; see Fig. 7. Specifically, the fluctuation function is determined^{41,45} using the time-series profile $Y(i) = \sum_{k=1}^i (r(t_k) - \langle r \rangle)$, which is then divided into non-overlapping segments of the length $n \in [2, T_{max}/4]$; the process is done once starting from the beginning of the time series and again starting from its end, thus resulting in $2N_s = 2Int(T_{max}/n)$ segments.

For each segment $\mu = 1, 2, \dots, N_s$ the local trend $y_\mu(i)$ is determined by using an interpolation procedure, and the standard deviation around that trend is defined as $F^2(\mu, n) = \frac{1}{n} \sum_{i=1}^n [Y((\mu - 1)n + i) - y_\mu(i)]^2$, and similarly $F^2(\mu, n) = \frac{1}{n} \sum_{i=1}^n [Y(N - (\mu - N_s)n + i) - y_\mu(i)]^2$ for $\mu = N_s + 1, \dots, 2N_s$ in the opposite direction. The q -th order fluctuation function $F_q(n)$ is then obtained

$$F_q(n) = \left\{ (1/2N_s) \sum_{\mu=1}^{2N_s} [F^2(\mu, n)]^{q/2} \right\}^{1/q} \sim n^{H_q} \quad (6)$$

for varied segment length n and its scale invariance investigated for a range of the values $q \in \mathcal{R}$. For each q value, the segments that appear to be scale-invariant (seen as straight lines in a double-log plot) are fitted to determine the corresponding scaling exponent H_q , defined in eq. (6). The spectrum of different generalised Hurst exponents expressed by the function H_q vs q

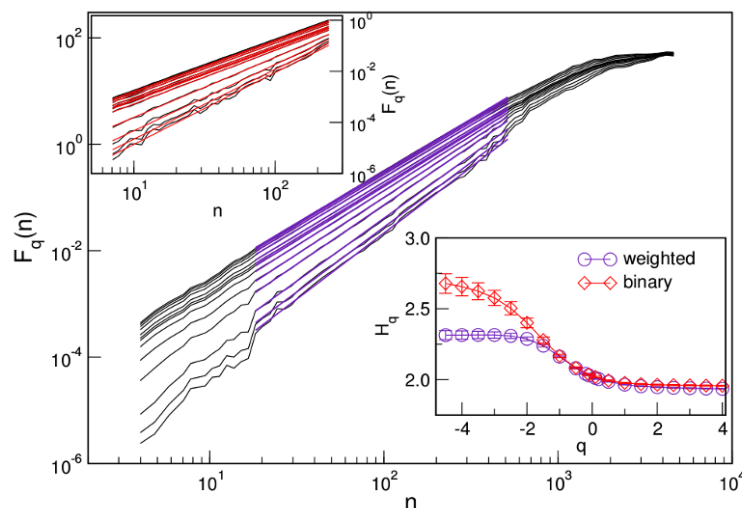


FIG. 7: The fluctuation function $F_q(n)$ vs time interval n for the order-parameter fluctuations in the instability region, $K_1 = 2.399$, shown in Fig. 4. Thick lines indicate the fitted region. The central panel shows the weighted core network's fluctuation function, while the binary network case is shown in the top inset. The corresponding generalised Hurst exponents H_q vs q are given in the bottom inset.

characterise the multifractal features of the time series, and we have $\Delta H = H_q^{max} - H_q^{min} > 0$, indicating how different segments of the time series need to be amplified differently to become self-similar to the rest of the data points. Here, we vary $q \in [-4.5, +4.5]$

such that H_q saturates in both limits. Thus, we examine the small-fluctuation segments, which are enhanced for the negative q values, and the large fluctuations segments that dominate the fluctuation function for the positive q values.

The results are given in Fig. 7, depicting the differences between the global phase fluctuations in the weighted and binary HC core networks. In particular, the fluctuation function $F_q(n)$ vs time interval n is shown with the corresponding scaling regions and the resulting multifractal spectra H_q vs q . Notably, at this point of the instability region, we have multifractal spectra with $\Delta H_q^B > \Delta H_q^W > 0$. Specifically, the spectra differ significantly at $q < 0$ side, corresponding to the enhanced small-scale fluctuations in the binary network, compared to the weighted counterpart. On the other side, the large fluctuations corresponding to $q > 0$ side of the spectra are of the same type and close to the fractional Brownian motion in both networks.

V. DISCUSSION AND CONCLUSIONS

Based on the human connectome core network, we presented a comprehensive methodology for analysing the multiscale oscillations of the global phase order parameter occurring in a range of positive couplings below the full synchrony threshold. We have expanded the previous study²⁶ of simulations of synchronisation processes by considering the cluster synchronisation with the Laplacian eigenvectors localisation and multifractal analysis of temporal evolution of the synchronisation order parameter. We demonstrated how these oscillations are linked to cluster synchronisation processes across a range of positive coupling strengths, all while remaining below the master stability threshold. An important aspect of our approach is based on spectral graph analysis of brain networks^{46,47} and eigenvector localization. It helps us locate clusters of nodes that play similar roles in synchronisation processes; these clusters are closely positioned within the eigenvector space. Consequently, we can identify the key clusters of brain regions and pinpoint the positions of hubs within these clusters. Furthermore, given the complexity of the network architecture we are working with, we carried out a parallel analysis of both the weighted core network and its binary version. It highlights the crucial role that the network's topology plays in forming synchronised clusters. Specifically, our results revealed that:

- Different synchronised clusters occur for a range of positive coupling strengths in the human connectome with the empirical weights and its binary version; this conclusion is supported by finding the connectome's spectral dimension is $d_s \approx 2.1$;
- Similarity of nodes identified in three major clusters surrounding brain hubs for weighted and binary network versions suggest the primary role of topology in the cluster synchronisation processes;
- Presence of these clusters causes multifractal fluctuations of the global phase order parameter, leading to different singularity spectra in the weighted and binary network version.

Several open questions remain for future study, in particular, given a complex higher-order structure of human connectome^{12,17} and the current trend of research in the synchronisation processes on higher-order networks^{48,49} and their applications in neurosciences^{18–20}. Particularly in contrast to interacting spin systems on simplicial complexes, where triangle-embedded interaction appears as another fundamental interaction inducing the collective (self-organised) state⁴⁹, the transition to a synchronised state is enabled solely by increased pairwise coupling strengths. Meanwhile, the higher-order interactions have an impact limited to the appearance of abrupt desynchronisation⁵⁰ and the shape of the hysteresis loop, depending on the dimension of the oscillators⁵¹ and size of simplexes in the simplicial complex, its architecture and the distribution of internal frequencies^{37,38}. Therefore, a nontrivial impact of higher-order interactions on the cluster synchronisation can be expected, in particular, in such complex structure, such as human connectome; this question remains to be investigated. We note that a different type of partial synchronisation exhibiting many small clusters due to frustration effects was observed for a broad range of negative pairwise couplings²⁶. There are still open questions regarding the differences in cluster synchronization between female and male connectomes, the resting state versus the active brain, and the recognition of brain disorders. We observe a certain degree of analogy in our approach to order-parameter-based multifractality analysis when studying cluster synchronization in human connectome core networks to spectral methodologies for other localization and delocalization phenomena, such as Anderson localization in complex systems. We also note that to the best of our knowledge, the first proposal for treating neuropathological conditions inspired by Anderson localization was introduced in⁵². The theoretical framework we have developed here opens new avenues for research in this direction.

In summary, we demonstrated how the topology around brain hubs critically shapes the global brain's dynamical coherence. In this context, cluster synchronisation plays a significant role in providing mechanisms for partial synchrony associated with the human connectome topology and quantified by the multifractal features of the global phase order parameter. In connection with empirical data, the study of these mechanisms can manifest further differences in brain function when processing specific tasks or deviations related to brain disorder pathways.

Acknowledgments

B.T. acknowledge the financial support from the Slovenian Research Agency under the program P1-0044. RM thanks the NSERC and the CRC Program for their support. MMD acknowledges funding provided by the Institute of Physics Belgrade, through the grant by the Ministry of Education, Science, and Technological Development of the Republic of Serbia. Numerical simulations were run on the PARADOX-IV supercomputing facility at the Scientific Computing Laboratory, National Center of Excellence for the Study of Complex Systems, Institute of Physics Belgrade.

-
- ¹ J. A. McNab, B. L. Edlow, T. Witzel, S. Y. Huang, H. Bhat, K. Heberlein, T. Feiweier, K. Liu, B. Keil, J. Cohen-Adad, M. D. Tisdall, R. D. Folkerth, H. C. Kinney, and L. L. Wald. The human connectome project and beyond: Initial applications of 300mt/m gradients. *NeuroImage*, 80:234 – 245, 2013. Mapping the Connectome.
 - ² Budapest reference connectome 3.0 <https://pitgroup.org/connectome/>
 - ³ B. Szalkai, C. Kerepesi, B. Varga, and V. Grolmusz. Parameterizable consensus connectomes from the human connectome project: the budapest reference connectome server v3.0. *Cognitive Neurodynamics*, 11(1):113–116, 2017.
 - ⁴ A. Avena-Koenigsberger, B. Misic, and O. Sporns. Communication dynamics in complex brain networks. *Nature Reviews Neuroscience*, 19:17, 2018.
 - ⁵ V. Zimmern. Why brain criticality is clinically relevant: A scoping review. *Front Neural Circuits*, art.54, 2020.
 - ⁶ C. Gros. A devil’s advocate view on ‘self-organized’ brain criticality. *J. Phys. Complexity*, 031001, 2021.
 - ⁷ S. Oldham and A. Fornito. The development of brain network hubs. *Developmental Cognitive Neuroscience*, 36:100607, 2019.
 - ⁸ V. Baruzzi, M. Lodi, F. Sorrentino, and M. Storace. Bridging functional and anatomical neural connectivity through cluster synchronization. *Scientific Reports*, 13:22430, 2023.
 - ⁹ L.L. Gollo, J.A. Roberts, V.L. Cropley, M.A. Di Biase., C. Pantelis, A. Breakspear, and M. Zalesky. Fragility and volatility of structural hubs in the human connectome. *Nature Neurosci*, 21:1107–1116, 2018.
 - ¹⁰ S. Achard, C. Delon-Martin, P. E. Vértes, F. Renard, M. Schenck, F. Schneider, C. Heinrich, S. Kremer, and E. T. Bullmore. Hubs of brain functional networks are radically reorganized in comatose patients. *Proceedings of the National Academy of Sciences*, 109(50):20608–20613, 2012.
 - ¹¹ C.J. Stam. Hub overload and failure as a final common pathway in neurological brain network disorders. *Netw Neurosci.*, 8(1):1–23, 2024.
 - ¹² B. Tadić, M. Andjelković, and R. Melnik. Functional geometry of human connectomes. *Sci. Rep.*, 9:12060, 2019.
 - ¹³ G. Petri, P. Expert, F. Turkheimer, R. Carhart-Harris, D. Nutt, P. J. Hellyer, and F. Vaccarino. Homological scaffolds of brain functional networks. *Journal of The Royal Society Interface*, 11(101):20140873, 2014.
 - ¹⁴ C. Pokorny, A. Ecker, J. Lazovskis, M. Santoro, J. P. Smith, K. Hess, R. Levi, and M. W. Reimann. Heterogeneous and higher-order cortical connectivity undergirds efficient, robust, and reliable neural codes. *iScience*, 28(1):111585, 2025.
 - ¹⁵ R. Hindriks, T. A. A. Broeders, M. M. Schoonheim, L. Douw, F. Santos, W. I van Wieringen, and P. K. B. Tewarie. Higher-order functional connectivity analysis of resting-state functional magnetic resonance imaging data using multivariate cumulants. *Human Brain Mapping*, 45(5):e26663, 2024.
 - ¹⁶ M. P. van den Heuvel and O. Sporns. Rich-club organization of the human connectome. *Journal of Neuroscience*, 31(44):15775–15786, 2011.
 - ¹⁷ M. Andjelković, B. Tadić, and R. Melnik. The topology of higher-order complexes associated with brain hubs in human connectomes. *Scientific Reports*, 10:17320, 2020.
 - ¹⁸ J.C. Pang, L.L. Gollo, and A.J. Roberts. Stochastic synchronization of dynamics on the human connectome. *NeuroImage*, 229:117738, 2021.
 - ¹⁹ M. Lodi, F. Della Rossa, F. Sorrentino, and M. Storace. Analyzing synchronized clusters in neuron networks, *Scientific Reports*, 10:16336, 2020.
 - ²⁰ C. I Anyaeji, J. Cabral, and D. Silbersweig. On a quantitative approach to clinical neuroscience in psychiatry: lessons from the kuramoto model. *Harvard Review of Psychiatry*, 29(4):318–326, 2021.
 - ²¹ A. K. Jaiswal and B. Bhushan Sharma. Cluster synchronization of networks of chaotic systems: A comprehensive review of theory and applications. *IETE Technical Review*, 41(5):537–556, 2024.
 - ²² X. Shi, X. Sun, Y. Lv, Q. Lu, and H. Wang. Cluster synchronization and rhythm dynamics in a complex neuronal network with chemical synapses. *Int J Non-Linear Mech*, 70, 2014.
 - ²³ Y. Qin, A. M. Nobili, D. S. Bassett, and F. Pasqualetti. Vibrational stabilization of cluster synchronization in oscillator networks. *IEEE Open Journal of Control Systems*, 2:439–453, 2023.
 - ²⁴ H. Fan, Y. Wang, and X. Wang. Eigenvector-based analysis of cluster synchronization in general complex networks of coupled chaotic oscillators. *Frontiers of Physics*, 18(4), 2023.
 - ²⁵ A. Bayani, F. Nazarimehr, S. Jafari et al. The transition to synchronization of networked systems. *Nat Commun*, 15:4955, 2024.
 - ²⁶ B. Tadić, M. Chutani, and N. Gupte. Multiscale fractality in partial phase synchronisation on simplicial complexes around brain hubs. *Chaos Solitons and Fractals*, 160:112201, 2022.
 - ²⁷ GP Pavlos, LP Karakatsanis, MN Xenakis, EG Pavlos, AC Iliopoulos, and DV Sarafopoulos. Universality of non-extensive tsallis statistics and time series analysis: Theory and applications. *Physica A: Statistical Mechanics and Its Applications*, 395:58–95, 2014.
 - ²⁸ M. Bastian, S. Heymann, and M. Jacomy. Gephi: An open source software for exploring and manipulating networks, 2009.

- ²⁹ S.N. Dorogovtsev, A.V. Goltsev, J.F. Mendes, and A.N. Samukhin. Spectra of complex networks. *Phys. Rev. E*, 68:046109, 2003
- ³⁰ M. Mitrovic Dankulov, B. Tadić, and R. Melnik. Spectral properties of hyperbolic nanonetworks with tunable aggregation of simplexes. *Phys. Rev. E*, 100:012309, 2019.
- ³¹ I. Seroussi and N. Sochen. Spectral analysis of a non-equilibrium stochastic dynamics on a general network. *Scientific Reports*, 8(1):14333, 2018.
- ³² A.P. Millan, J. Torres, and G. Bianconi. Synchronization in networks with finite spectral dimension. *Phys. Rev. E*, 99:022307, 2019.
- ³³ M. Mitrović and B. Tadić. Spectral and dynamical properties in classes of sparse networks with mesoscopic inhomogeneities. *Phys. Rev. E*, 80(2):026123, 2009.
- ³⁴ M. Newman. Spectral methods for community detection and graph partitioning. *Phys. Rev. E*, 88:042822, 2013.
- ³⁵ E. Andrade and G. Dahl. Combinatorial fiedler theory and graph partition. *Linear Algebra and its Applications*, 687(12):02.005, 2024.
- ³⁶ L. Zhao and L. Sawlani, S. and Akoglu. Density of states for fast embedding node-attributed graphs. *Knowl Inf Syst*, 65:2455–2483, 2023.
- ³⁷ M. Chutani, B. Tadić and N. Gupte. Hysteresis and synchronization processes of kuramoto oscillators on high-dimensional simplicial complexes with competing simplex-encoded couplings. *Phys. Rev. E*, 104:034206, Sep 2021.
- ³⁸ S. Sahoo, B. Tadić, and N. Gupte. Effect of hidden geometry and higher-order interactions on the synchronization and hysteresis behavior of phase oscillators on 5-clique simplicial assemblies. *Phys. Rev. E*, 108:034309, 2023.
- ³⁹ L. V. Gambuzza, F. Di Patti, L. Gallo, S. Lepri, M. Romance, R. Criado, M. Frasca, V. Latora, and S. Boccaletti. *The Master Stability Function for Synchronization in Simplicial Complexes*, pages 249–267. Springer International Publishing, Cham, 2022.
- ⁴⁰ A.N. Pavlov and V. S. Anishchenko. Multifractal analysis of complex signals. *Physics–Uspekhi*, 50:819–834, 2007.
- ⁴¹ J. W. Kantelhardt, S. A. Zschiegner, E. Koscielny-Bunde, S. Havlin, A. Bunde, and H.E. Stanley. Multifractal detrended fluctuation analysis of nonstationary time series. *Physica A: Statistical Mechanics and its Applications*, 316:87 – 114, 2002.
- ⁴² M Sadegh Movahed, G R Jafari, F Ghasemi, S. Rahvar, and M Reza Rahimi Tabar. Multifractal detrended fluctuation analysis of sunspot time series. *Journal of Statistical Mechanics: Theory and Experiment*, 2006(02):P02003, 2006.
- ⁴³ J. Hu, J. Gao, and X. Wang. Multifractal analysis of sunspot time series: the effects of the 11-year cycle and fourier truncation. *Journal of Statistical Mechanics: Theory and Experiment*, 2009(02):P02066, 2009.
- ⁴⁴ S. Drozd and P. Oswiecimka. Detecting and interpreting distortions in hierarchical organization of complex time series. *Phys. Rev. E*, 91:030902(R), 2015.
- ⁴⁵ B. Tadić. Multifractal analysis of barkhausen noise reveals the dynamic nature of criticality at hysteresis loop. *Journal of Statistical Mechanics: Theory and Experiment*, 2016(6):063305, 2016.
- ⁴⁶ Robinson, Peter A and Henderson, James A and Gabay, Natasha C and Aquino, Kevin M and Babaie-Janvier, Tara and Gao, Xiao. Determination of dynamic brain connectivity via spectral analysis. *Frontiers in Human Neuroscience*, 15:655576, 2021.
- ⁴⁷ A. Bobyleva, A. Gorsky, S. Nechaev, O. Valba, and N. Pospelov. Metric structural human connectomes: Localization and multifractality of eigenmodes. *Network Neuroscience*, 1-30:00439, 2025.
- ⁴⁸ P.K. Pal, Md S. Anwar, M. Perc, and D. Ghosh. Global synchronization in generalized multilayer higher-order networks. *Phys. Rev. Res.*, 6:033003, 2024.
- ⁴⁹ B. Tadić and R. Melnik. Fundamental interactions in self-organised critical dynamics on higher order networks. *The European Physical Journal B*, 97(6):68, 2024.
- ⁵⁰ P. S. Skardal and A. Arenas. Abrupt desynchronization and extensive multistability in globally coupled oscillator simplexes. *Phys. Rev. Lett.*, 122:248301, 2019.
- ⁵¹ X. Dai, K. Kovalenko, M. Molodyk, Z. Wang, X. Li, D. Musatov, A.M. Raigorodskii, K. Alfaro-Bittner, G.D. Cooper, G. Bianconi, and S. Boccaletti. D-dimensional oscillators in simplicial structures: Odd and even dimensions display different synchronization scenarios. *Chaos, Solitons & Fractals*, 146:110888, 2021.
- ⁵² J B. J. Zhang, M. Chamanzar, and M.-R. Alam. Suppression of epileptic seizures via Anderson localization. *J Royal Soc Interface*, 14(127):20160872, 2017.